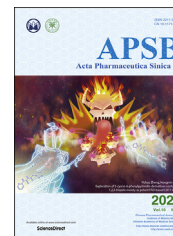




Chinese Pharmaceutical Association
Institute of Materia Medica, Chinese Academy of Medical Sciences

Acta Pharmaceutica Sinica B

www.elsevier.com/locate/apsb
www.sciencedirect.com



ORIGINAL ARTICLE

Functional nano-vector boost anti-atherosclerosis efficacy of berberine in *Apoe*^(-/-) mice



Xiaolei Ma^{a,†}, Tingting Zhang^{a,†}, Zhigang Luo^a, Xiaolin Li^a,
Miao Lin^a, Rui Li^a, Peng Du^a, Xiaoyou Yu^a, Chen Ma^{a,b}, Pengju Yan^b,
Jin Su^b, Lulu Wang^{a,*}, Yuhuan Li^{c,*}, Jiandong Jiang^{a,c}

^aState Key Laboratory of Bioactive Substance and Function of Natural Medicines, Beijing City Key Laboratory of Drug Delivery Technology and Novel Formulations, Institute of Materia Medica, Chinese Academy of Medical Sciences and Peking Union Medical College, Beijing 100050, China

^bDepartment of Pharmacy, Jiamusi University, Jiamusi 154007, China

^cInstitute of Medicinal Biotechnology, Chinese Academy of Medical Sciences and Peking Union Medical College, Beijing 100050, China

Received 7 November 2019; received in revised form 9 February 2020; accepted 12 March 2020

KEY WORDS

Atherosclerosis;
Berberine;
Functional nano-vector;
Endothelial activation

Abstract Atherosclerosis (AS) is the leading cause of heart attacks, stroke, and peripheral vascular disease. Berberine (BBR), a botanical medicine, has diversified anti-atherosclerotic effects but with poor absorption. The aim of this study was to develop an effective BBR-entrapped nano-system for treating AS in high-fat diet (HFD)-fed *Apoe*^(-/-) mice, and also explore the possible underlying mechanisms involved. Three D- α -tocopherol polyethylene glycol (PEG) succinate (TPGS) analogues with different PEG chain lengths were synthesized to formulate BBR-entrapped micelles. HFD-fed *Apoe*^(-/-) mice were administered with optimized formula (BBR, 100 mg/kg/day) orally for 5 months. The artery plaque onset and related metabolic disorders were evaluated, and the underlying mechanisms were studied. Our data showed that, BT₁₅₀₀M increased BBR deposition in liver and adipose by 107.6% and 172.3%, respectively. In the *Apoe*^(-/-) mice, BT₁₅₀₀M ameliorated HFD-induced hyperlipidemia and lipid accumulation in liver and adipose. BT₁₅₀₀M also suppressed HFD-induced chronic inflammation as evidenced by the reduced liver and adipose levels of interleukin-6 (IL-6), tumor necrosis factor- α (TNF- α) and interleukin-1 β (IL-1 β); and decreased plasma level of TNF- α , IL-6, IL-1 β , interferon- γ (IFN- γ), monocyte chemoattractant protein (MCP), and macrophage inflammatory factor (MIP). The mechanism study showed

*Corresponding authors. Tel./fax: +86 10 63017757.

E-mail addresses: wanglulu@imm.ac.cn (Lulu Wang), yuhuanlibj@126.com (Yuhuan Li).

[†]These authors made equal contributions to this work.

Peer review under responsibility of Chinese Pharmaceutical Association and Institute of Materia Medica, Chinese Academy of Medical Sciences

<https://doi.org/10.1016/j.apsb.2020.03.005>

2211-3835 © 2020 Chinese Pharmaceutical Association and Institute of Materia Medica, Chinese Academy of Medical Sciences. Production and hosting by Elsevier B.V. This is an open access article under the CC BY-NC-ND license (<http://creativecommons.org/licenses/by-nc-nd/4.0/>).

that BT₁₅₀₀M changed *Ampk* and *Nf-κb* gene expression, and interrupted a crosstalk process between adipocytes and macrophages. Further investigation proved that BT₁₅₀₀M decreased endothelial lesion and subsequent macrophage activation, cytokines release, as well as cholesteryl ester gathering in the aortic arch, resulting in ameliorated artery plaque build-up. Our results provide a practical strategy for treating AS using a BBR-entrapped nano-system.

© 2020 Chinese Pharmaceutical Association and Institute of Materia Medica, Chinese Academy of Medical Sciences. Production and hosting by Elsevier B.V. This is an open access article under the CC BY-NC-ND license (<http://creativecommons.org/licenses/by-nc-nd/4.0/>).

1. Introduction

Atherosclerosis (AS) is by far the single most important pathological process in the development of cardiovascular diseases (CVDs) and responsible for more than 75% of all deaths due to CVDs¹. AS begins with endothelial damage. Dysregulation of lipid metabolism and aberrant inflammatory responses are considered major risk factors for AS². Despite the use of statins (lipid-lowering drugs) in clinical treatments, many problems remain because of the limited action of these drugs on sub-clinical risk factors other than lipid metabolism³. In addition, typical side effects such as myopathy (which may progress to rhabdomyolysis statin-associated muscle symptoms), gastrointestinal disorders, renal damage, liver function impairment, and fatigue have been frequently reported and recognized as the main causes of statin discontinuation⁴. Moreover, the European Society of Cardiology Guidelines states that statins might increase the incidence of diabetes, especially in older patients and those with other diabetes risk factors⁵. Aspirin is an important agent applied in the treatment and long-term prevention of CVDs. However, recent research revealed that aspirin shows only modest benefit and is not recommended for those over age of 70. Furthermore, the United States Preventive Services Task Force recommends against the use of aspirin for prevention of CVDs in women less than 55 years and men less than 45 years of age, as the risk of serious bleeding is almost equal to the benefit with respect to cardiovascular problems^{6,7}. Therefore, there is an urgent need to find complementary and alternative medicines for patients with a high risk of AS. Recently, berberine (BBR), an isoquinoline derivative alkaloid [molecular weight (MW) 235.32 Da] extracted from medicinal herbs, has drawn increasing attention. It is an approved nutraceutical compound for the treatment of variety of metabolic disorders^{8,9}. Its safety and tolerability for long-term applications have been supported by epidemiological data¹⁰. In the past decade, accumulating studies have demonstrated the anti-atherosclerotic effect of BBR in multiple phases with diverse mechanisms, including recuperation of dyslipidemia, alleviation of inflammatory processes and improvement of endothelial dysfunction¹¹. In addition, the affirmative effects of BBR against metabolic diseases, such as diabetes and insulin resistance¹⁰, liver diseases¹² and obesity¹³, which are the high-risk factors for atherogenesis, have been acknowledged. BBR has the potential to be a promising medicine for palliating AS. However, the efficacy of BBR in treating AS should be further improved for its clinical application.

The absolute bioavailability of BBR after oral administration has been reported to be below at 1%¹⁴. Therefore, several approaches have been explored to increase its bioavailability^{15,16}. However, its further translation into therapeutic intervention was hindered by inefficient studies on pharmacodynamics and

mechanisms. D- α -Tocopherol polyethylene glycol succinate (TPGS) is a water-soluble derivative of natural vitamin E (VE, D- α -tocopherol) formed by the esterification of VE succinate with polyethylene glycol (PEG). TPGS-based nano delivery systems show promise in improving drug absorption through their abilities to reduce aggregation¹⁷, increase solubility, and enhance permeability of the entrapped agents. TPGS also acts as a P-glycoprotein (P-gp) inhibitor to improve the oral bioavailability and cellular uptake of many drugs¹⁸. TPGS has been approved by the U.S. Food and Drug Administration (FDA) as a safe pharmaceutical adjuvant, and VE was reported to benefit AS treatment¹⁹. TPGS nano-system is considered to have unique advantages on BBR delivery and possess a synergistic effect with BBR in the treatment of AS²⁰. Previous studies demonstrated that the P-gp-inhibiting and permeation-enhancing abilities of TPGS-based micelles were related to the length of their tethering chains^{18,21}; TPGS with 1000–2000 PEG chains were the most studied ones^{19,20,22}. Therefore, in this study, three TPGS analogs with a range of PEG chain lengths (400, 1500, and 3000 Da) were synthesized to formulate a BBR-entrapped nano-system. The optimized BBR formula was verified for its anti-atherogenic efficacy in *Apoe*^(-/-) mice, and the underlying molecular mechanism of this system was intensively explored *in vitro* and *in vivo*. In the present study, we aimed to enhance the anti-atherosclerotic efficacy of BBR by using FDA-approved functional biomaterial TPGS as a carrier and elucidate its therapeutic effect and underlying molecular.

2. Materials and methods

D- α -Tocopherol, succinate, PEG (MW 400, 1500 and 300 Da), triethylamine (TEA), 4-dimethylaminopyridine (DMAP), *N,N'*-dicyclohexylcarbodiimide (DCC) and phosphate buffered saline (PBS, pH 7.4) were purchased from Sigma–Aldrich (St. Louis, MO, USA). BBR was obtained from J&K Scientific Ltd. (Beijing, China). Trypsin-EDTA (0.25%), cell culture media, penicillin/streptomycin and FBS were obtained from Thermo Fisher Scientific (Waltham, MA, USA). All other reagents were of analytical grade. All water used in the study was freshly double distilled.

3T3-L1, HepG2 and Caco2 cell lines were obtained from the Cell Resource Center, Peking Union Medical College (head quarter of National Infrastructure of Cell Line Resource, NSTI, Beijing, China).

Male *Apoe*^(-/-) mice (6 weeks, 20–22 g) were purchased from Charles River (Beijing, China). The *in vivo* study was approved by the Laboratories' Institutional Animal Care and Use Committee of the Chinese Academy of Medical Sciences (Beijing, China), and the research was conducted in accordance with the guidelines and ethics of the Chinese Council on Animal Care (project identification code 00005970).

2.1. Synthesis and characterization of TPGS analogues

The procedure for the synthesis of α -tocopherols succinate was adapted from Abu-Fayyad et al.²³ and described in Supporting Information.

2.2. Preparation and characterization of BBR-TPGS micelles

The preparation and characterization of BBR-TPGS micelles were described by Miet et al.¹⁹ and Bisht et al.²⁴ The details were included in Supporting Information.

2.3. Bio-distribution of orally administered BBR formulations in *ApoE*^(-/-) mice

Different BBR containing micelles were administered to *ApoE*^(-/-) mice by gavage (100 mg/kg/day of BBR). At each preset time point, five mice for each group were euthanized. The blood samples were gathered from posterior orbital venous plexus to a heparinized tube. The major organs (heart, liver, lung and adipose) were harvested and immediately immersed in liquid nitrogen and stored at -80°C . The distribution of BBR in various formulations was also analyzed by LC-MS/MS (Shimadzu LC-20AD-UFLC, Kyoto, Japan) described previously²⁵.

2.4. Cell culture and treatment

The procedure of cell culture and treatment was described in Supporting Information.

2.5. In vivo study

ApoE^(-/-) mice were fed with HFD (high-fat diet) accompanied with pure BBR (BP), BT₁₅₀₀M (BM) or empty micelle (EV) for 5 months. Untreated HFD-fed mice were used as model control (MC) while *ApoE*^(-/-) mice fed with standard chow diet as negative control (NC). At the end of the experiments, ¹H-MRS spectrum and MRI were conducted to analyze fat accumulation. Then the mice were anesthetized after 12 h fasting period. Plasma was collected for biochemical and cytokine analyses. The tissues of liver, epididymis fat and arterial arch were harvested and weighed. All tissues were divided into two parts, one was fixed with 10% formalin, and the remaining one was immediately immersed in liquid nitrogen and stored at -80°C for further analysis. The procedure of *in vivo* analysis was described in Supporting Information.

3. Results

3.1. Synthesis and characterization of TPGS analogues

The ¹H NMR (500 Hz; Varian, Palo Alto, CA, USA) spectra and FT-IR (Nicolet5700, Madison, USA) spectra of D- α -tocopherol, PEG, succinate, and TPGS are shown and described in Supporting Information (Supporting Information Fig. S1).

3.2. Preparation and characterization of BBR-TPGS micelles

The characterizations of BBR-TPGS micelles are shown and described in Supporting Information (Supporting Information Figs. S2 and S3).

3.3. Bio-distribution of orally administered BBR formulations in *ApoE*^(-/-) mice

Effective drug delivery to the target sites is a prerequisite for disease therapy. The bio-distribution properties of BT₁₅₀₀M (BM) and pure BBR (BP) were verified by LC-MS/MS analysis described previously^{25,26}. As shown in Supporting Information Fig. S4 and Tables S1 and S2, BBR had a high distribution in tissues such as the liver and fat. Notably, deposition of active BBR in the liver and fat was found to be increased dramatically in BT₁₅₀₀M-treated mice compared with that in BP-treated mice whereas BBR organ distribution property was not changed by the nano delivery system. The enhanced active drug deposition in the BM group was consistent with the results of *in vitro* Caco2 transwell permeability assay and cellular uptake experiments. This phenomenon could be due to improved gut absorption and enhanced cellular uptake of BBR assisted by the micelles. Although increase in liver drug deposition was also found in the BT₄₀₀M and BT₃₀₀₀M-treated group, it was not as significant as that in the BT₁₅₀₀M group (data not show), agreeing with previous studies which demonstrated that the length of the PEG chain in TPGS could influence the P-gp-inhibiting and permeation-enhancing ability of TPGS micelles. As liver and adipose tissues are active participants in whole body energy homeostasis and inflammation, they were proved to play important roles in AS treatment. The improved liver and adipose deposition of BBR might benefit its therapeutic effect. BBR was undetectable in the arterial arch.

3.4. Pharmacodynamics study

Owing to the marked characteristics of BT₁₅₀₀M *in vitro*, we studied its effect *in vivo* and explored the underlying mechanisms. *ApoE*^(-/-) mice fed HFD were divided into 4 groups. These groups received PBS (MC), BP, BM, or empty vector (EV), respectively for 5 months *via* gavage. *ApoE*^(-/-) mice fed standard chow diet were used as negative control (NC).

3.4.1. BT₁₅₀₀M intervention results in improvement of endothelial injury and consequent inflammation process

AS is a multistep disease of the arterial wall, alteration of the function and structural integrity of the endothelial barrier precede the formation of plaques²⁷. The expression levels of ICAM-1 and VCAM-1, the two crucial adhesion molecules, were determined in the aortas of experimental mice. The results show that 5 months of HFD feeding upregulated the expression of ICAM-1 and VCAM-1 in the aortas of *ApoE*^(-/-) mice (Fig. 1 and Supporting Information Fig. S5A), which is in agreement with the results of previous research²⁸. In contrast, the expression of ICAM-1 and VCAM-1 was significantly decreased in the aortas of mice in BM group. A slight decline in the expression of these molecules was observed in BP mice. An improvement in the expression of ICAM-1 and VCAM-1 was observed in EV mice, but the difference was not statistically significant. The expression of different cytokines including TNF- α , IL-6, monocyte chemoattractant protein 1 (MCP-1), and matrix metalloproteinase 9 (MMP9) was further tested. As shown in Figs. 1C, 2A and 2B, a substantial increase in these cytokines was detected in the aortic arch of MC mice compared with that of NC mice. Treatment of HFD-fed *ApoE*^(-/-) mice with BT₁₅₀₀M greatly inhibited these increases. A mild decline in these cytokines was observed in BP mice and EV mice, but the differences were not statistically significant.

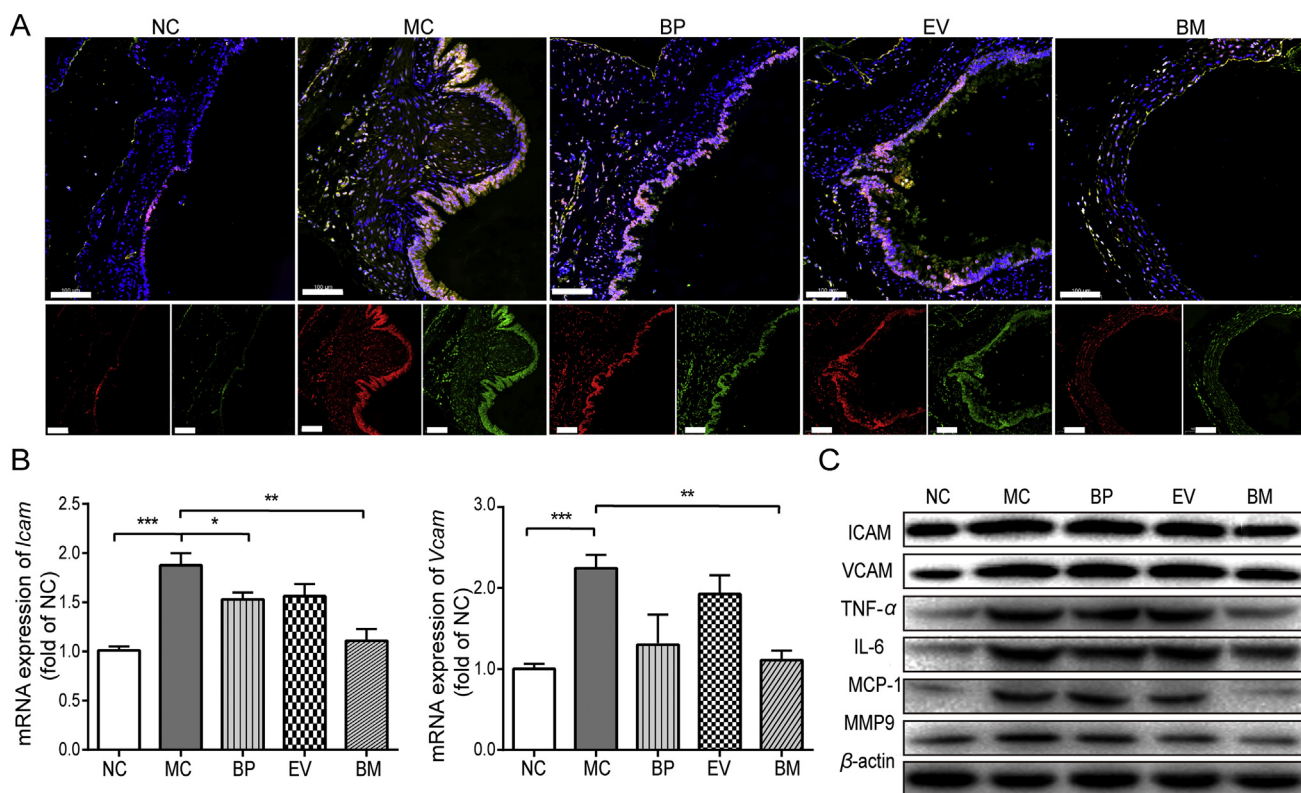


Figure 1 $BT_{1500}M$ decreases endothelial injury in atherosclerotic lesion. $Apoe^{(-/-)}$ mice were fed with HFD accompanied with pure BBR (BP), $BT_{1500}M$ (BM) or empty vector (EV) for 5 months. Untreated HFD-fed mice were used as model control (MC) while $Apoe^{(-/-)}$ mice fed with standard chow diet were used as negative control (NC). At the end of experiment, the aortas from $Apoe^{(-/-)}$ mice in different group were collected. (A) Representative adhesive molecule expression. Atherosclerotic lesions in the aortic sinuses from $Apoe^{(-/-)}$ mice in different group were stained for ICAM (red), VCAM (green) and DAPI (blue). (B) The mRNA expression of *Icam* and *Vcam* was evaluated by RT-PCR. The results were normalized to *Gapdh*. (C) The protein expression of ICAM, VCAM, MCP-1, MMP9, IL-6 and TNF- α was tested using Western blot analysis. The results were normalized to β -actin. Data are presented as mean \pm SEM ($n = 6$), * $P < 0.05$, ** $P < 0.01$, *** $P < 0.001$, vs. mice in MC group. Scale bars, 100 μ m (A).

3.4.2. $BT_{1500}M$ ameliorate arterial plaque

$Apoe^{(-/-)}$ mice have been well recognized to develop a robust aortic atherosclerotic phenotype when fed with HFD¹⁹. The severity of aortic AS in HFD-fed $Apoe^{(-/-)}$ mice was evaluated after treatment with different reagents. As shown in Fig. 3, HFD-fed mice developed more aortic lesions than chow diet-fed mice. Notably, $BT_{1500}M$ -treatment significantly reduced the severity of atherosclerotic lesions in the aortic arch of HFD-fed $Apoe^{(-/-)}$ mice. A dramatic increase in cholesteryl (CE) gathering was found in the aortic artery of MC mice compared with that of NC mice (Fig. S5B). Treatment of HFD-fed $Apoe^{(-/-)}$ mice with $BT_{1500}M$ greatly inhibited CE content. A mild alleviation of atherosclerotic lesions and CE gathering was also detected in BP mice and EV mice.

3.5. Mechanism study

The liver plays central role in nutrients metabolism. As energy storage site, adipose tissue has been recognized as a major endocrine organ which secret many pro-inflammatory cytokines, thereby inducing a chronic systemic inflammatory response²⁹. Previous studies of us and others proved that, liver and adipose are the target site for BBR on metabolic diseases^{30–32}. Tissue

distribution analysis showed that $BT_{1500}M$ improved BBR deposition in the liver and adipose. Therefore, we further explored the molecular mechanisms and interpreted the therapeutic effect of $BT_{1500}M$ on AS, taking liver and adipose as target tissues.

3.5.1. $BT_{1500}M$ modulated the expression of NF- κ B and AMPK in the liver and fat tissues

Multiple target pathways have been identified for verifying the anti-dyslipidemic and anti-inflammatory effects of BBR, among which AMP-activated protein kinase (AMPK) and nuclear factor kappa B (NF- κ B) play pivotal roles. The expression of NF- κ B and AMPK in the liver and fat tissues was examined by immunofluorescence (IF) staining (C2t Nikon fluorescent microscope, Tokyo, Japan) as well as quantitative RT-PCR (ABI 7500 Fast, Foster, USA) and Western blot (Bio Rad, Hercules, CA, USA) analyses. As shown in Fig. 4A and B, HFD significantly increased NF- κ B expression in the liver and adipose of $Apoe^{(-/-)}$ mice compared with standard chow diet. $BT_{1500}M$ -treated mice showed amplified levels of p-AMPK and decreased levels of NF- κ B in liver and fat tissues compared with MC group. The gene-modulating effect of $BT_{1500}M$ was further confirmed by Western blot and RT-PCR (Fig. 4C–E) analyses. The effect was also observed in BP, but it was less pronounced. In EV-treated mice,

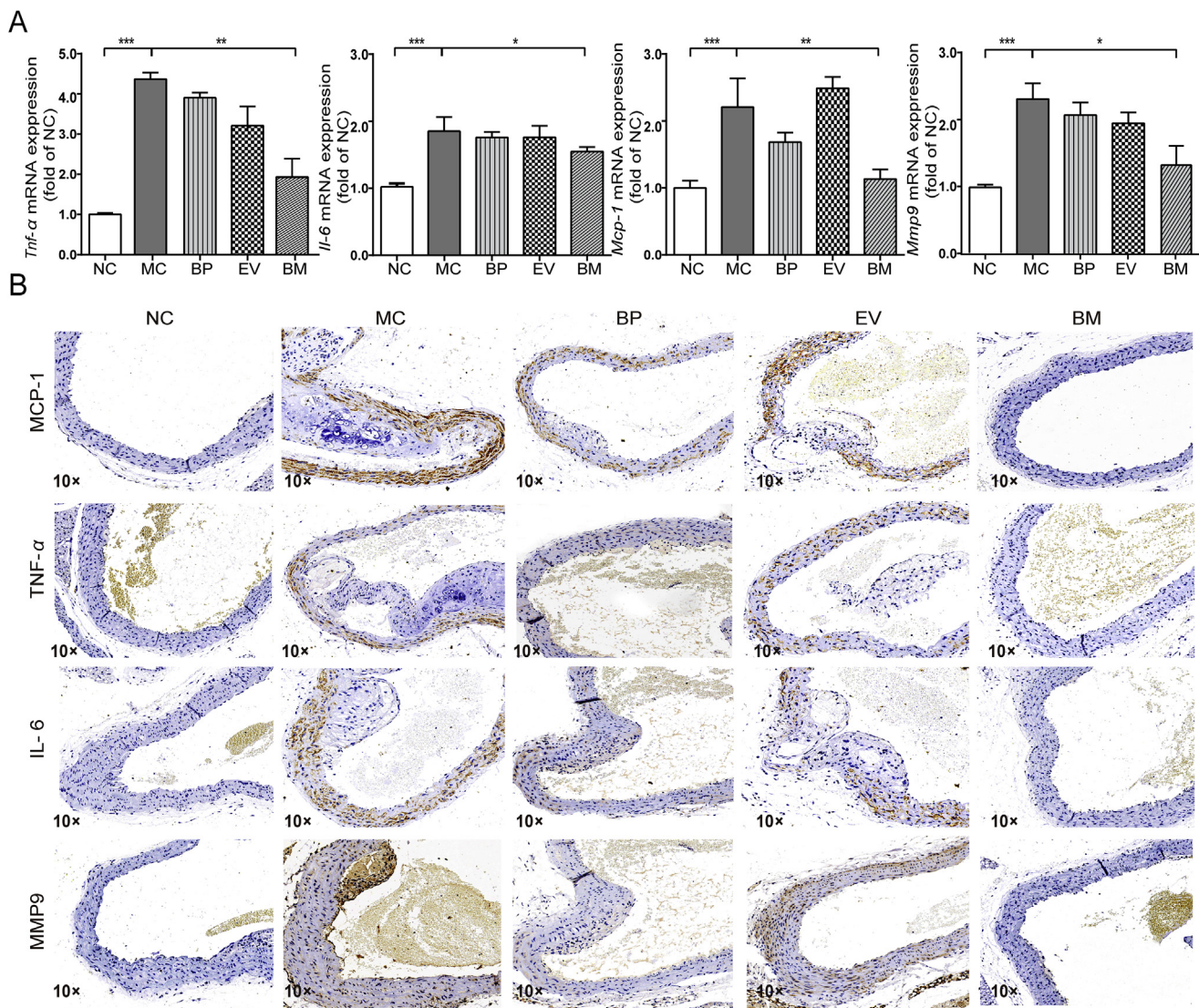


Figure 2 BT₁₅₀₀M alleviated arterial inflammation. HFD-fed *ApoE*^(-/-) mice treated with various BBR formulations (100 mg/kg/day of BBR) by gavage. Untreated HFD-fed mice were used as model control while *ApoE*^(-/-) mice fed with standard chow diet were used as negative control. At the end of experiment, the aortas from *ApoE*^(-/-) mice in different group were collected. (A) The mRNA expression of *Tnf-α*, *Il-6*, *Mcp-1* and *Mmp9* was evaluated by RT-PCR. The results were normalized to *Gapdh*. (B) Representative protein expression of MCP-1, TNF-α, IL-6 and MMP9 visualized by ICH staining. Data are presented as mean ± SEM (*n* = 6), **P* < 0.05, ***P* < 0.01, ****P* < 0.001, vs. mice in MC group.

no effect on p-AMPK was detected, while NF-κB was found to be down-regulated.

3.5.2. BT₁₅₀₀M alleviated hyperlipidemia and metabolic disorders in HFD-fed *ApoE*^(-/-) mice

We first evaluated the therapeutic effect of BT₁₅₀₀M on hyperlipidemia. As shown in Fig. 5A, after 5 months of treatment, the plasma levels of total cholesterol (TC), triglyceride (TG), and low-density lipoprotein-cholesterol (LDL-c) in MC mice were significantly higher than those in NC mice. However, the plasma levels of TC, TG, and LDL-c in HFD-fed mice treated with BT₁₅₀₀M drastically decreased compared with those in the MC group. No significant difference in HDL-c levels was found among all groups. BP was also found to ameliorate plasma lipid levels but to a lesser extent. No change was found in the plasma lipid levels of mice after treatment with EV. An increase in subcutaneous fat,

liver index, and epididymis fat index was observed in MC group compared with that in NC mice. Although BT₁₅₀₀M treatment improved these disorders, the difference between treated and untreated groups was not statistically significant (Fig. 5B and C), representative MRI images tested using Pharma Scan 70/16 US small animal MRI (Bruker, Karlsruhe, Germany). No drastic difference in AST and ALT levels was found among all tested animals (Fig. 5D). The images of whole body, liver, and epididymis fat in experimental animals are shown in Fig. 5E.

3.5.3. BT₁₅₀₀M suppressed lipid accumulation and ROS generation in the liver

As shown in Fig. 6A, the livers in MC group showed numerous spherical vacuoles. The accumulation of large lipid droplets was verified by Oil Red O staining (Fig. 6B). BM intervention markedly decreased hepatocyte lipid accumulation. A decrease in lipid

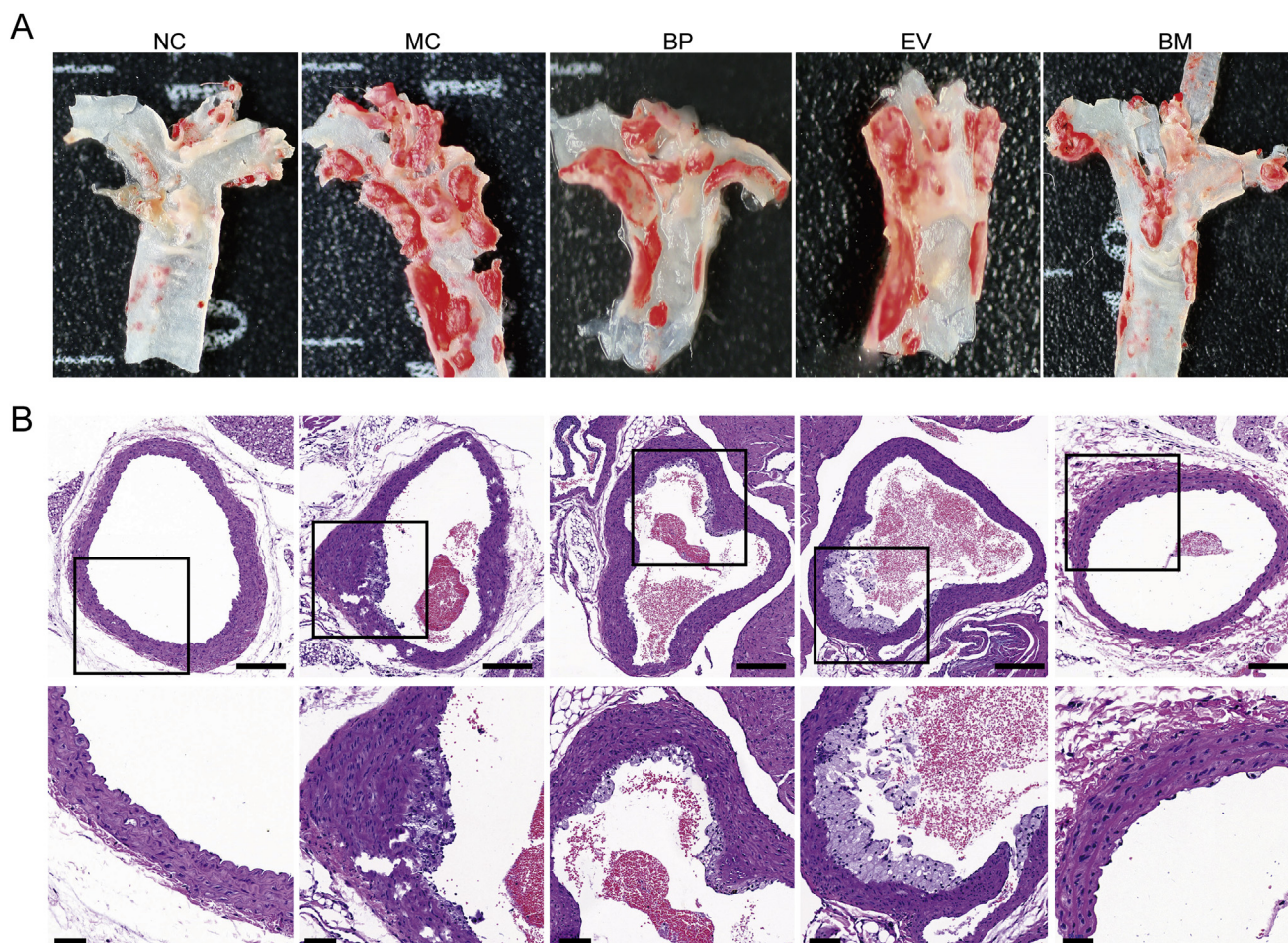


Figure 3 BT₁₅₀₀M ameliorated arterial plaque formation. HFD-fed *Apoe*^(-/-) mice treated with various BBR formulations (100 mg/kg/day of BBR) by gavage. Untreated HFD-fed mice were used as model control while *Apoe*^(-/-) mice fed with standard chow diet were used as negative control. (A) Representative images of oil red-stained aortic arch lesion in *Apoe*^(-/-) mice. (B) Representative images of HE-stained cross-sections of the aorta in *Apoe*^(-/-) mice. Scale bars 200 μ m (B, up) and 50 μ m (B, down).

droplet accumulation was detected in BP administered mice, but the magnitude was lower than that in BM mice. No significant change was found in EV-treated animals compared with that in MC group. In addition, ROS production induced by HFD was greatly inhibited after BT₁₅₀₀M exposure (Fig. 6C and D). Consistent with the *in vivo* evaluation, *in vitro* experiment on HepG2 cells verified that the increase in ROS production and inflammatory factors induced by saturated fatty acids was inhibited by BT₁₅₀₀M (Supporting Information Fig. S6). Mild anti-ROS and anti-inflammatory effects were detected in BP-treated cells. Notably, a decline in inflammatory cytokine levels was observed in vector-treated HepG2 cells with less ROS production. Among all the tested groups, BT₁₅₀₀M showed the best benefits against palmitic acid (PMA)-stimulated ROS production and inflammatory response. The enhanced effects of BT₁₅₀₀M might be attributed to the conjunction effect.

3.5.4. BT₁₅₀₀M inhibited lipid accumulation and interrupted a crosstalk process between adipocytes and macrophages

Adipose tissue macrophage (ATM) activation plays an important role in the development of low-grade chronic inflammation. It was proved that hypertrophic enlarged adipocytes tend to release altered adipocytokines, initiating the macrophage infiltration and

polarization. Polarized type 1 macrophages (M1) release more inflammatory cytokines which in turn activate the inflammatory response in adipocytes and macrophages. This chronic inflammation was then propagated by this feed-forward process^{33,34}. We first examined the effect of BT₁₅₀₀M treatment on fat accumulation in adipose tissues. As can be seen in Fig. 7A, MC group showed an increase in adipocyte size relative to NC mice. BT₁₅₀₀M medication restored adipocyte size to that of NC mice. Adipocyte size in BP mice was smaller than that in MC mice. No significant difference in adipocyte size was found in EV and MC mice. The effect of BBR formulation on macrophage infiltration and M1 type macrophage activation was explored. As illustrated in Fig. 7B, F4/80⁺ cells, which represent macrophages, increased in HFD-fed mice compared with that in normal chow-fed mice. F4/80⁺/CD86⁺ cells, which represent M1, also significantly increased (Fig. 7C). A significant increase in the expression of *Inos* and *Il-12* (M1) was detected in adipose tissues of HFD-fed mice compared with that of NC group (Fig. 7D). After treatment with BT₁₅₀₀M, the number of F4/80⁺ macrophages that infiltrated into the adipose of *Apoe*^(-/-) mice significantly decreased compared to untreated mice. The number of F4/80⁺/CD86⁺ cells and expression of *Inos* and *Il-12* decreased after BT₁₅₀₀M intervention. BP and EV showed milder modulatory effects on macrophage activation than BM did.

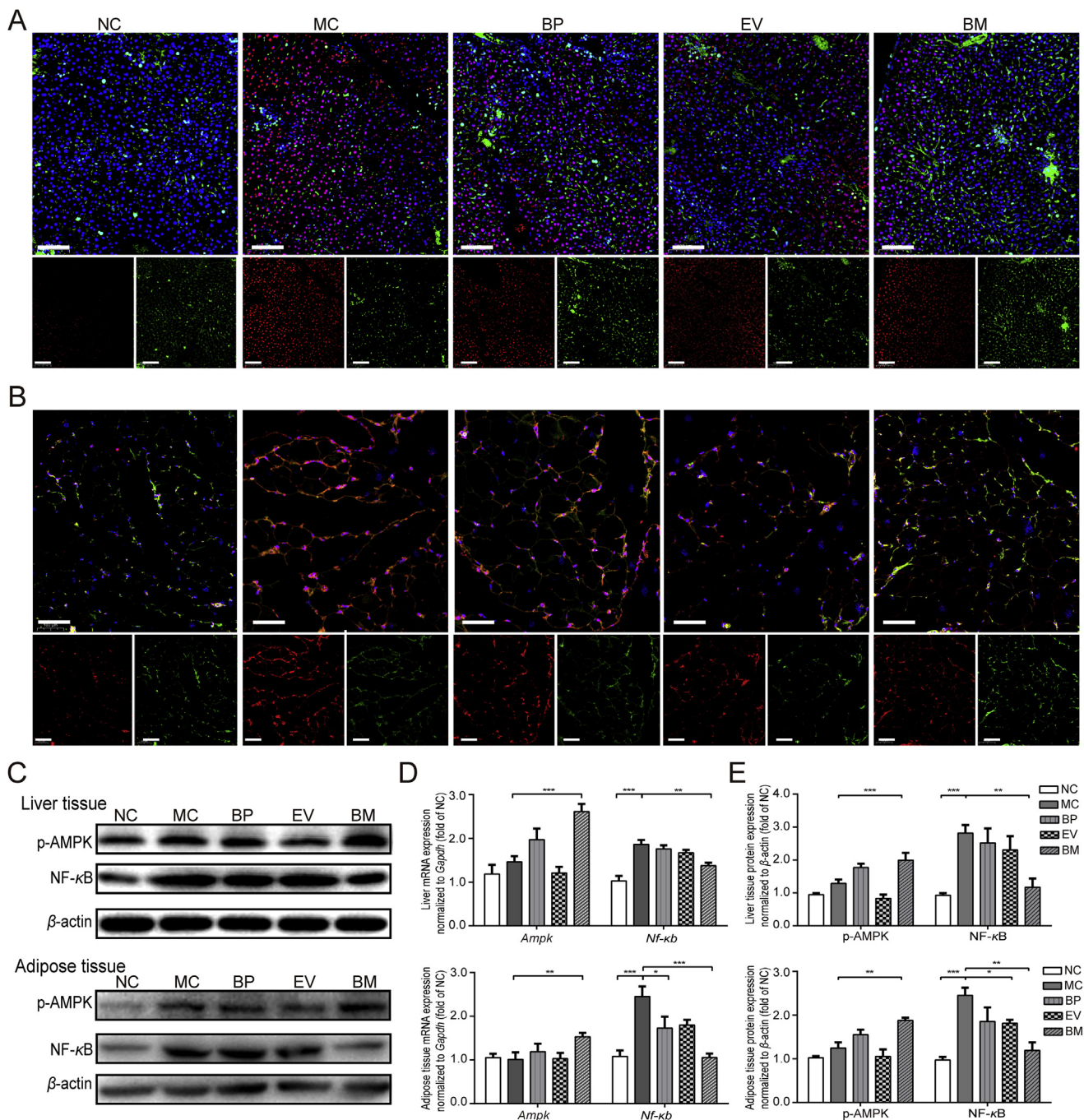


Figure 4 BT₁₅₀₀M modulated the expression of AMPK and NF- κ B in *Apoe*^(-/-) mice fed with HFD. HFD-fed *Apoe*^(-/-) mice treated with various BBR formulations (100 mg/kg/day of BBR) by gavage. Untreated mice fed with standard rodent diet (NC) were used as control. (A) Representative photographs of p-AMPK (green) and NF- κ B (red) protein expression in liver tissue of different group mice visualized using C2t Nikon fluorescent microscope by probing with anti-p-AMPK and NF- κ B antibodies simultaneously. (B) Representative photographs of p-AMPK (green) and NF- κ B (red) protein expression in adipose of different group mice visualized using C2t Nikon fluorescent microscope by probing with anti-p-AMPK and NF- κ B antibodies simultaneously. (C) The protein expression of p-AMPK and NF- κ B was tested using Western blot analysis. The result was normalized to β -actin. (D) The mRNA expression of *Ampk* and *Nf- κ B* was evaluated by RT-PCR. The results were normalized to *Gapdh*. (E) The semi-quantitative analysis of Western blot data. Data are presented as mean \pm SEM ($n = 6$), * $P < 0.05$, ** $P < 0.01$, *** $P < 0.001$, vs. mice in MC group. Scale bars, 100 μ m (A) and (B).

The effect of BT₁₅₀₀M on macrophage activation was verified *in vitro*. First, we detected whether the effect of BBR formulation on adipocytes would modulate chemotaxis of macrophages using *in vitro* chemotaxis transwell migration assay (24-well plates, 8 μ m

pore size, Corning, Lowell, MA, USA). As described in the experiment section, RAW 264.7 cells were incubated with conditioned medium collected from 3T3-L1 cells stimulated with PAM presented with BBR formulations or vectors. As shown in

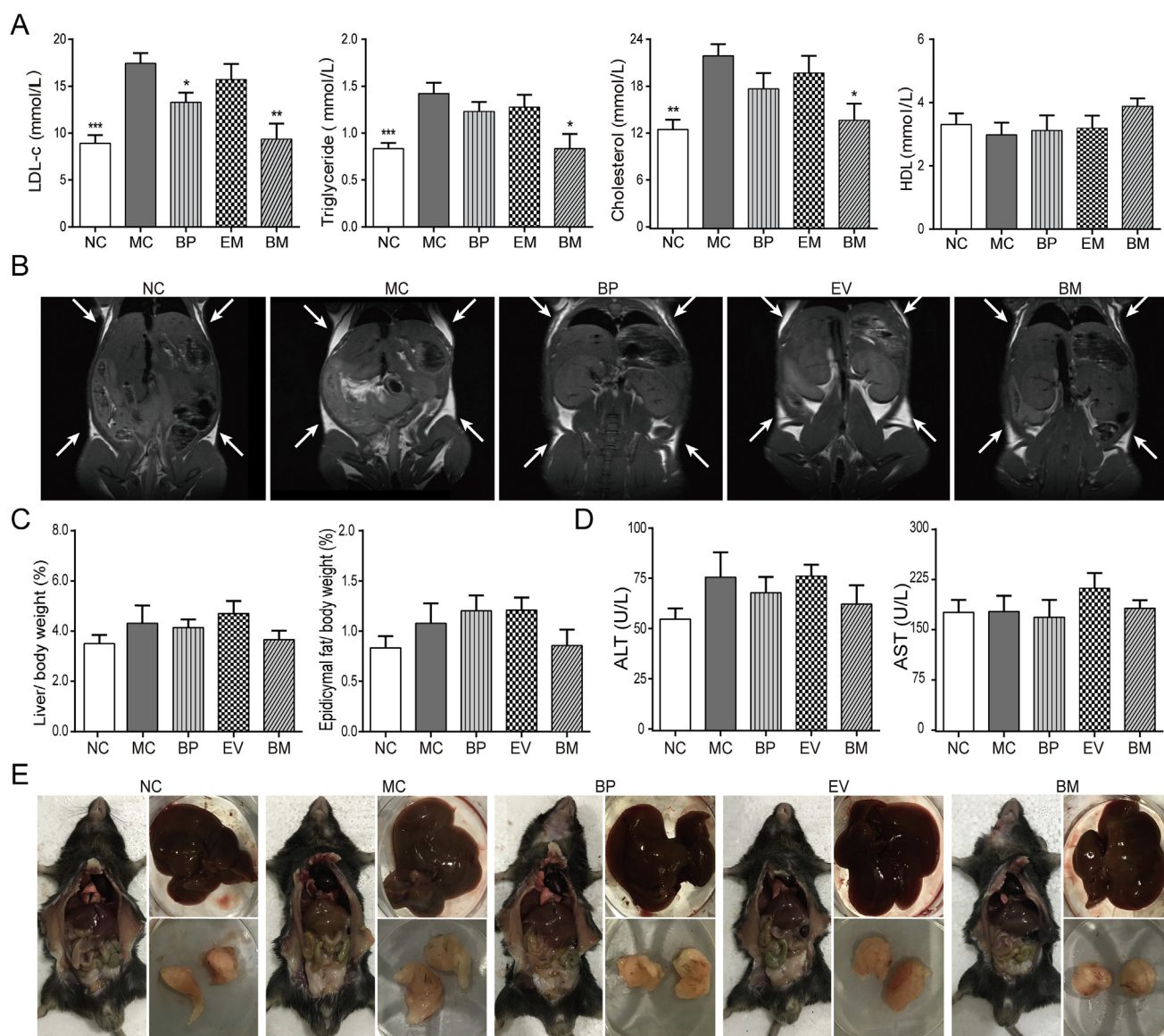


Figure 5 *In vivo* pharmacodynamic analysis HFD-fed *ApoE*^(-/-) mice were treated with various BBR formulations by gavage. Untreated mice fed with HFD (MC group); and standard rodent diet (NC group) were used as control. (A) Plasma lipid analyses. Plasma TG, cholesterol, LDL-c and HDL were measured with enzymatic methods using an automatic biochemical analyzer. (B) Representative MRI images tested using Pharma Scan 70/16 US small animal MRI. White arrow points subcutaneous fat. (C) Liver and epididymis fat index. (D) ALT and AST level analyses. (E) Representative pictures of whole body, liver tissue and epididymal fat. Data are presented as mean \pm SEM ($n = 6$), * $P < 0.05$, ** $P < 0.01$, *** $P < 0.001$, vs. mice in MC group.

Supporting Information Fig. S7A, the migration of RAW 264.7 macrophages was highly enhanced by the conditioned medium collected from adipocytes treated with PAM, and this phenomenon was suppressed by BT₁₅₀₀M treatment. Next, we evaluated the effect of BBR formulations on macrophage polarization. RAW 264.7 macrophages were incubated with LPS alone or combined with BBR formulations, and the expression of M1 phenotype was determined. Flow cytometry (BD FACSVerser, Franklin, USA) analysis showed that the number of CD11c⁺/CD86⁺ cells significantly increased in LPS-treated cells than in solvent-treated ones (Supporting Information Fig. S7B). Furthermore, LPS induced a significant increase in the expression of *Il-6*, *Il-12* and *Tnf- α* , and a decrease in the expression of *Il-10* in RAW 264.7 cells (Figs. S7C and D). After treatment with BT₁₅₀₀M, the number of CD11c⁺/CD86⁺ cells significantly decreased

compared to untreated RAW 264.7 macrophages stimulated with LPS. BP and EV groups showed mild modulatory effects on M1 activation. Among the different treatments, BT₁₅₀₀M showed optimal efficacy. The improved effect of BT₁₅₀₀M on macrophage infiltration and activation might be attributed to the synergistic effect of BBR and vector as well as improved cellular uptake³⁵. These results implied that BT₁₅₀₀M successfully inhibited the trigger of macrophage activation and interrupted the crosstalk process between adipocytes and macrophages, which might contribute to its anti-inflammatory effect.

3.5.5. BT₁₅₀₀M improved inflammation status in HFD-fed *ApoE*^(-/-) mice

Chronic inflammation is a major contributing factor to AS. Compelling evidence has suggested that various markers of

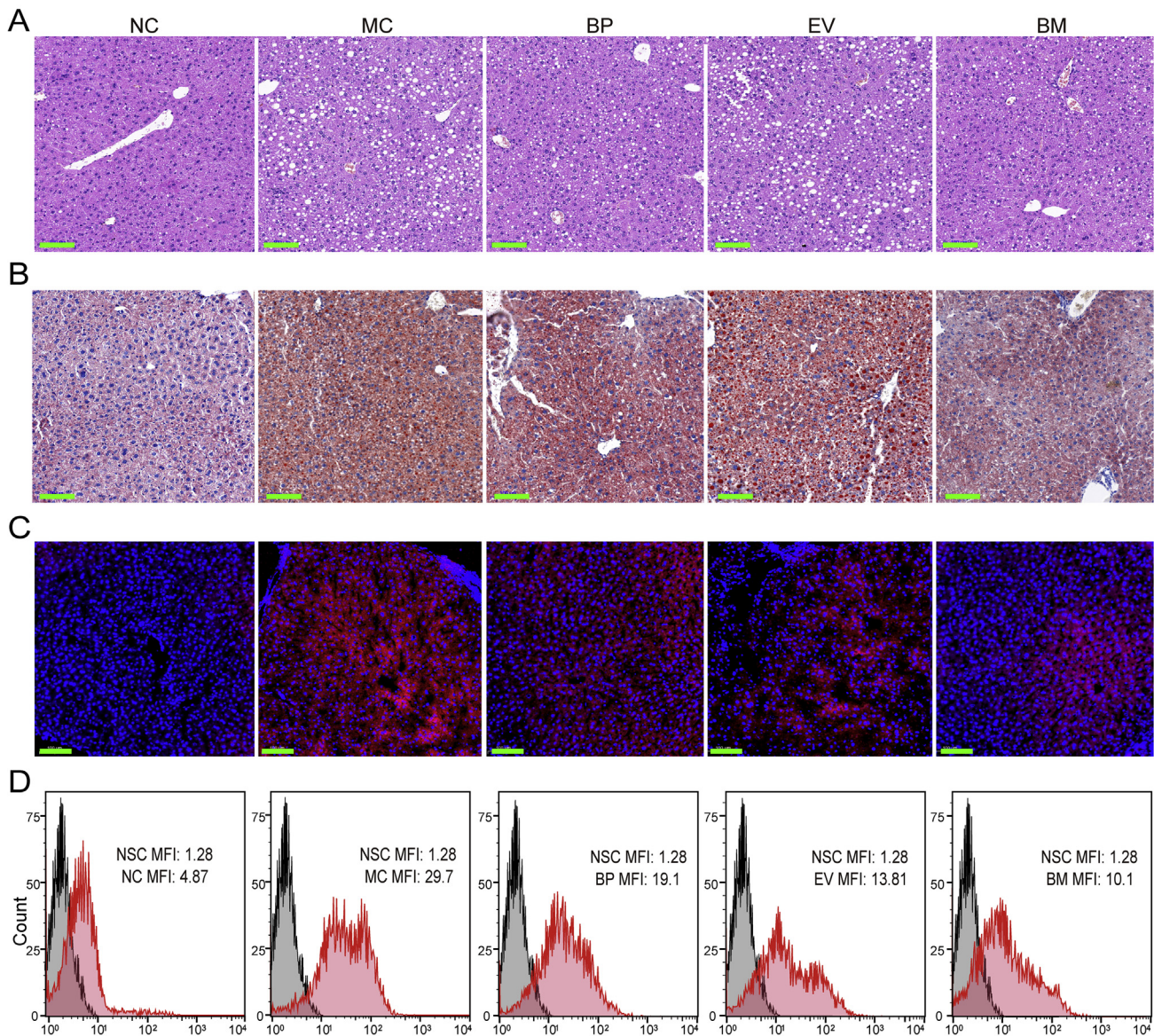


Figure 6 BT₁₅₀₀M suppressed lipid accumulation and ROS production in liver. *Apoe*^(-/-) mice were fed with HFD accompanied with pure BBR (BP), BT₁₅₀₀M (BM) or empty vector (EV) for 5 months. Untreated HFD-fed mice were used as model control (MC) while *Apoe*^(-/-) mice fed with standard chow diet were used as negative control (NC). At the end of experiment, the liver tissues from *Apoe*^(-/-) mice in different group were collected. (A) Representative photograph of HE-stained liver sections. (B) Representative photographs of oil red-stained liver sections. (C) Representative fluorescent images of fluorescence in liver tissue visualized using C2t Nikon fluorescent microscope; ROS production was measured using a fluorescent probe, H2DCFDA. (D) Representative Flow cytometry diagrams of ROS in isolated liver cells. Scale bars, 100 μ m (A), (B) and (C). Representative fluorescent images of fluorescence in liver tissue visualized using C2t Nikon fluorescent microscope; ROS production was measured using a fluorescent probe, H2DCFDA. (D) Representative Flow cytometry diagrams of ROS in isolated liver cells. Scale bars, 100 μ m (A), (B) and (C).

inflammation are upregulated in patients with established atherosclerotic disease and the pro-inflammatory cytokines were associated with endothelial dysfunction and important in response to AS and valvular lesion. In this study, proinflammatory factors in tissues and circulation were investigated. As shown in Fig. 8A and B, NC mice expressed low levels of TNF- α , IL-6, and IL-1 β in the liver and adipose tissues, whereas the levels of these factors increased in MC mice. BT₁₅₀₀M intervention significantly reduced the expression of these proinflammatory factors. The mRNA expression levels of proinflammatory cytokines, including IL-1 β , IL-6 and TNF- α , markedly reduced in the

liver and adipose tissues in BM mice compared to those in MC mice. The results of Western blot analysis were consistent with those of RT-PCR. The above findings suggest that BT₁₅₀₀M treatment successfully alleviated inflammation in *Apoe*^(-/-) mice fed HFD. BP exposure tended to reduce the levels of IL-6, IL-1 β , and TNF- α in both hepatic and adipose tissues, with a magnitude lesser than that of BM group. Notably, HFD-fed mice treated with EV showed decreased IL-6, IL-1 β and TNF- α level in fat and liver tissues, but the differences were not statistically significant. Ten inflammatory cytokines in the circulation were further investigated. As shown in Fig. 8C, a substantial increase in TNF-

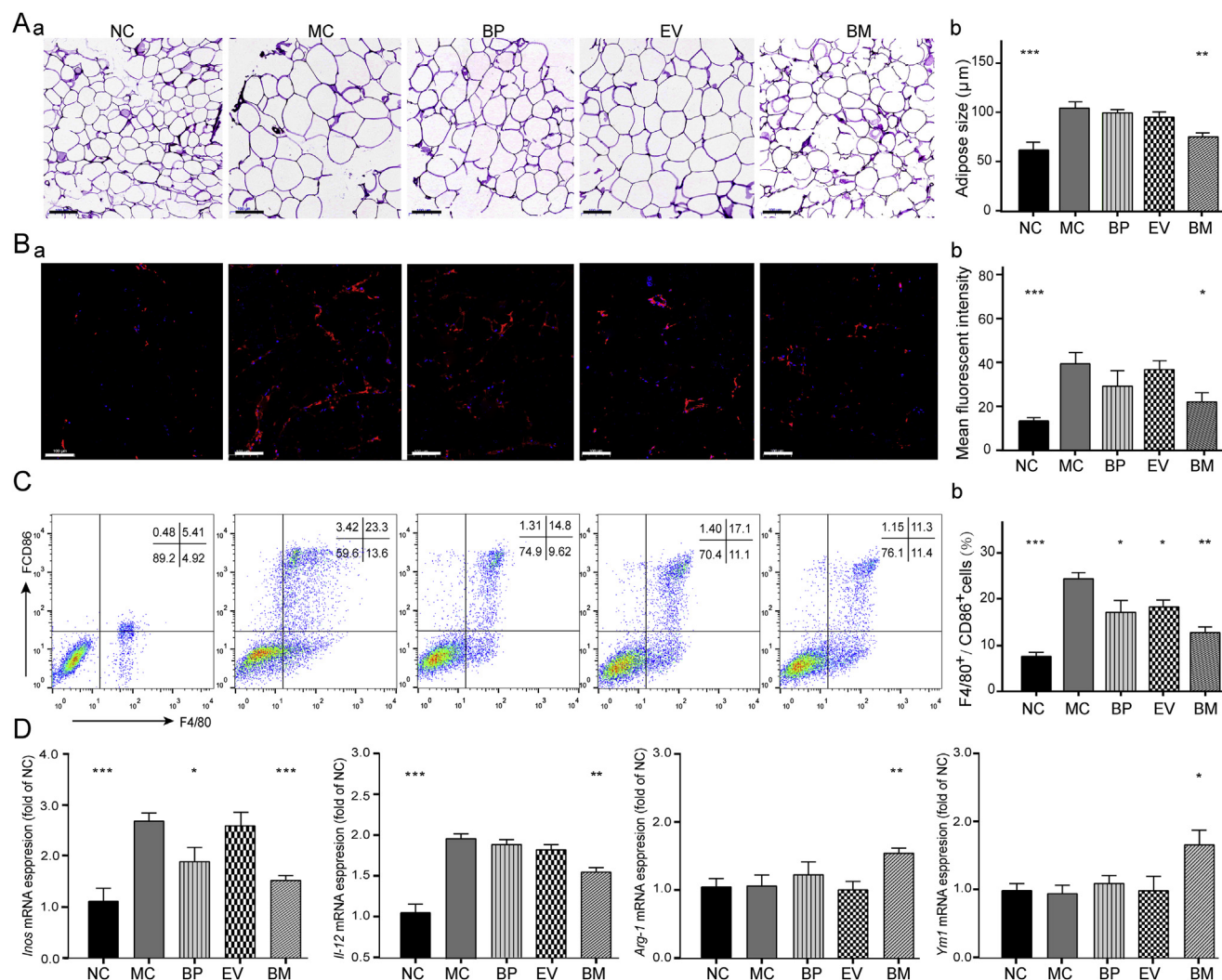


Figure 7 BT₁₅₀₀M reduced lipid accumulation, inhibited macrophages infiltration and activation in fat tissue. *ApoE*^(-/-) mice was fed with HFD accompanied with pure BBR (BP), BT₁₅₀₀M (BM) or empty vector (EV) for 5 months. Untreated HFD-fed mice were used as model control (MC) while *ApoE* knock-out mice fed with standard chow diet were used as negative control (NC). At the end of experiment, the epididymis fat from *ApoE*^(-/-) mice in different group were collected. (A)-a, representative photograph of HE-stained epididymis fat sections; (A)-b, mean adipocyte size of epididymis fat. (B)-a, macrophage infiltration was visualized with C2t Nikon fluorescent microscope after staining for macrophages marker F4/80; (B)-b, mean fluorescent intensity (MFI) of PE. (C)-a, epididymal fat stromal vascular cells were isolated and M1 macrophages were analyzed by flow cytometry after staining with PE-conjugated anti-F4/80 antibody and APC-conjugated anti-CD86 antibody; (C)-b, percentage of F4/80⁺/CD86⁺ cells. (D) Total RNA was extracted from epididymis fat and analyzed by quantitative real-time PCR for *Inos*, *Il-12* (M1 phenotype marker) and *Arginase1*, *Ym1* (M2 phenotype marker) the results were normalized to *Gapdh*. Data are presented as mean ± SEM (*n* = 5), **P* < 0.05, ***P* < 0.01, ****P* < 0.001, vs. mice in MC group. Scale bars, 100 μm (A) and (B).

α , IL-1 β , IFN- γ , MCP, MIP, and IL-6 production was detected in the plasma of MC mice compared with that of NC mice by enzyme linked immunosorbent assay (ELISA; R&D Systems, MN, USA) according to instruction of the manufacturer. However, treatment of HFD-fed *ApoE*^(-/-) mice with BM greatly inhibited this elevation. A decline in these cytokines was also observed in BP mice and EV mice, but the magnitudes were lower than that in BM-treated mice.

3.6. In vivo safety

Long-term safety was investigated to examine the biocompatibility of BT₁₅₀₀M. *ApoE*^(-/-) mice received BT₁₅₀₀M (100 mg/kg/day of BBR, *n* = 5) for 5 months by gavage administration, and untreated

mice were used as controls. As shown in Supporting Information Fig. S8, no obvious histological difference was found between the major organs of treated and untreated mice. No significant differences in plasma levels of ALT, AST, creatinine, and blood urea nitrogen were found between the two groups, implying good safety and tissue compatibility of BT₁₅₀₀M.

3.7. Statistical analysis

Data were expressed as the mean ± standard error means (SEM). Values measured by the two folds of standard deviation were discarded. Statistical analysis was performed in GraphPad Prism Software Version 5.0a (GraphPad, San Diego, CA, USA) using unpaired Student's *t*-test.

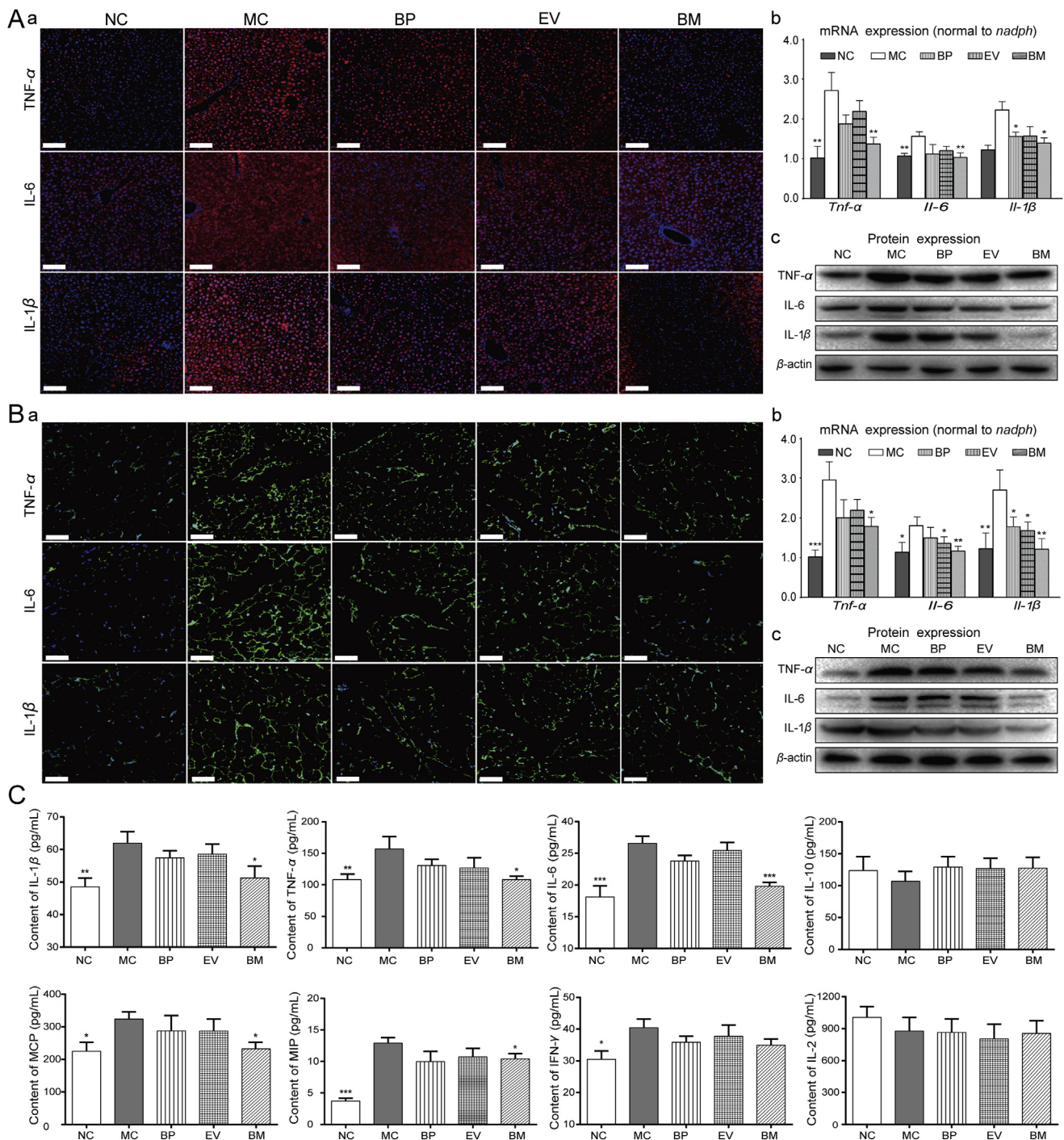


Figure 8 BT₁₅₀₀M improved inflammation status in HFD-fed *Apoe*^(-/-) mice. HFD-fed *Apoe*^(-/-) mice treated with various BBR formulations by gavage. The tissue of epididymal fat and liver were harvested. (A)-a, representative photograph of immuno-fluorescent stained liver tissues for IL-6, IL-1β or TNF-α visualized using C2t Nikon fluorescent microscope; (A)-b, the expression of *Il-6*, *Il-1β* and *Tnf-α* mRNA in liver tissue were evaluated by RT-PCR. The results were normalized to *Gapdh*; (A)-c, the protein expression of IL-6, IL-1β and TNF-α in liver tissue was evaluated by Western blot, β-actin used as control. (B)-a, representative photographs of immuno-fluorescent stained adipose tissues for IL-6, IL-1β or TNF-α visualized using C2t Nikon fluorescent microscope; (B)-b, the expression of *Il-6*, *Il-1β* and *Tnf-α* mRNA in adipose tissue were evaluated by RT-PCR. The results were normalized to *Gapdh*; (B)-c, the protein expression of IL-6, IL-1β and TNF-α in adipose was evaluated by Western blot, β-actin used as control. (C) Pro-inflammation cytokine levels in plasma. Following the termination of the experiment, blood samples were collected and used for the determination of plasma TNF-α, IL-1β, IL-6, IL-2, IL-10, MCP-1, MIP and IFN-γ levels by ELISA according to instruction of the manufacturer. Data are presented as mean ± SEM (*n* = 6). **P* < 0.05, ***P* < 0.01, ****P* < 0.001, vs. mice in MC group. Scale bars, 100 μm (A) and (B).

4. Discussion

In this study, the nano delivery system BT₁₅₀₀M was developed for improving the anti-atherosclerotic efficacy of BBR. The bioactivity of BT₁₅₀₀M was elucidated *via* intensive studies on its formulation properties, organ distribution, and molecular mechanism. The results demonstrated that *Ampk* and *Nf-κb* gene expressions, which are crucial for energy homeostasis and inflammation, were extensively modulated because of improved drug deposition and drug-carrier synergism. In *ApoE*^(-/-) mice, BT₁₅₀₀M effectively ameliorated dyslipidemia and inflammation induced by HFD feeding. Endothelial injury, subsequent macrophage accumulation, and cholesteryl ester gathering in the aortic arch site were reduced, resulting in the inhibition of artery plaque build-up. BT₁₅₀₀M exhibited a better therapeutic effect on HFD-induced AS than BP or EV did, with no apparent toxicity.

AS is a disease in which the inside of an artery narrows due to the build-up of plaque. The build-up of an atheromatous plaque is a complex process developed through a series of cellular events, and in response to various local vascular and circulating factors. Endothelial injury has been recognized to be the first and essential step for AS. It favours following cell adhesion and migration, lipids deposition, monocytes invasion and differentiation into macrophage, smooth muscle cells transfer into the intima, as well as further damaging the vasculature, propagating plaque erosion and augmenting thrombus formation³¹. Accumulating evidence confirms that endothelial dysfunction is associated with LDL particles and chronic inflammation. Dyslipidemia and chronic inflammation induce an increase in the expression of *Icam-1* and *Vcam-1* in endothelial cells, making it more adhesive to monocytes and other effectors in the circulation for trans-endothelial recruitment. The blood-derived monocytes transmigrate through the endothelium then extravagate into the intima, and hence differentiates into macrophage. In the intima, macrophage proliferated and engulfed ox-LDL through receptor-mediated process, resulting in a series of highly regulated, albeit maladaptive cellular events which drive the atherogenic response. Increased secretion of cytokines including TNF- α , IL-6, MCP-1, and MMP9 induce the expression of scavenger receptors on macrophages, resulting in the accumulation of large amounts of cholesteryl esters and formation of foam cells that appear as a fatty streak²⁷.

BBR is a promising candidate for AS treatment owing to its pleiotropic anti-dyslipidemic and anti-inflammatory effects. In 2004, our team first discovered BBR, a new lipid-lowering drug with a novel mechanism compared to statins. The anti-inflammatory activity of BBR was observed both *in vitro* and *in vivo* *via* reduction of proinflammatory cytokines and acute phase proteins^{36,37}. BBR treatment has been shown to reduce the production of TNF- α , IL-6, IL-1 β , MMP9, cyclooxygenase-2, inducible nitric oxide synthase, MCP-1, C-reactive protein, and haptoglobin in cultured adipocytes, liver cells, macrophages, splenocytes, and pancreatic β -cells. *In vivo* research proved that BBR can reduce proinflammatory cytokines in different tissues such as the serum, liver, adipose, and kidneys³⁸. Furthermore, clinical study has shown that BBR therapy at a dose of 1 g/day for 3 months significantly reduced serum IL-6 levels in patients with type 2 diabetes mellitus³⁹. AMPK and NF- κ B are main targets in the molecular mechanism underlying the anti-metabolic and anti-inflammatory effects of BBR⁴⁰. As an energy gauge⁴¹, AMPK plays a crucial role in the regulation of fatty acid oxidation⁴², lipid metabolism⁴³, and cholesterol synthesis^{43,44}. Numerous recent

studies have implicated a key role for NF- κ B signaling pathway in the liver, adipose tissue, and central nervous system in the development of inflammation-associated metabolic diseases⁴⁵. BBR has been proved to reduce inflammation-induced NF- κ B overexpression^{46,47}. However, the efficacy of BBR for AS treatment needs to be improved.

We previously designed a liver-target system for boosting the effect of BBR on cardio-metabolic diseases²⁶. However, its clinic application is still in its infancy because of the tedious examination and approval procedures for new materials. In this study, TPGS was selected for BBR delivery, and its effect on AS treatment and the molecular mechanism of the system were intensively explored. In recent years, many research groups have concentrated on various applications of TPGS as drug delivery vehicles in nanomedicine, among which micelles have unique advantages⁴⁸. TPGS-based micelles effectively reduced the aggregation of drugs in circulation and simulated body fluid, enhanced the permeability in the gut intestinal tract, and increased intracellular uptake of entrapped reagents^{17,18}. A wide range of drug-containing micelles such as camptothecin⁴⁹, paclitaxel⁵⁰, quercetin⁵¹, and cetuximab⁵¹ have been successfully investigated. Three TPGS analogs were synthesized in this study to formulate BBR-entrapped nano-system. Our results showed that BT₁₅₀₀M formed stable micelles in aqueous vehicles at low concentrations with high encapsulation efficiency. This nano-system could increase gut absorption and intracellular uptake of BBR, leading to increased active drug deposition in the liver and adipose site.

The organ distribution property of pharmaceuticals can help elucidate the possible molecular mechanism. Previous studies by us and others^{30,31} proved that the liver and adipose are the target sites for BBR on metabolic diseases. The liver plays a central role in nutrient metabolism (especially lipid), including cholesterol synthesis, lipogenesis, TG production; a bulk of the body's lipoproteins are synthesized in the liver. Adipose tissue, which is known as an energy storage site (in the form of lipids), has recently been recognized as a major endocrine organ as it produces hormones such as, estrogen, resistin, and cytokines. Adipose tissue macrophage activation plays an important role in the development of low-grade chronic inflammation. Hypertrophic enlarged adipocytes tend to release altered adipocytokines, initiating macrophage infiltration and polarization. Polarized macrophages release more inflammatory cytokines which in turn activate inflammatory response in adipocytes and macrophages. In adipose tissue, an increased secretion of various adipose tissue-derived proinflammatory cytokines leads to local effects on white adipose tissue; these effects also extend to tissues such as the liver, where they can stimulate hepatic inflammation¹³ and produce many acute phase proteins, inducing a chronic systemic inflammatory response²⁹. Chronic inflammation, a major contributing factor to AS, is then propagated by this feed-forward process^{33,34}. In this study, the time-dependent *in vivo* bio-distribution of BBR was monitored using LC-MS/MS method after gavage administration of BBR-containing formulations in *ApoE*^(-/-) mice. Improved accumulation of BBR in the liver and fat tissues was found in BT₁₅₀₀M-treated animals compared with mice treated with BP. This was consistent with the findings of previous studies^{14,27}. Notably, this nano-system did not change the organ distribution profile of BBR, but strengthened BBR retention in tissues. TPGS might reduce drug efflux, thus leading to improved drug accumulation and therapeutic efficacy. Although an increase in liver drug deposition was also found in BT₄₀₀M- and BT₃₀₀₀M-treated groups, it was not as significant as that in the

BT₁₅₀₀M group (data not shown). This finding is in agreement with that of previous studies, which demonstrated that the length of PEG chain in TPGS could influence the P-gp-inhibiting and permeation-enhancing ability of TPGS micelles. Collnot et al.¹⁸ demonstrated that PEG length (200–6000) of TPGS could inhibit the activity of efflux pump. The promising TPGS derivatives are TPGS with PEG 1100–1500. Zhao et al.²¹ suggested that the high surface energy of micelles formed by TPGS with PEG chain lengths between 1000 and 1500 can overcome the bending energy needed to penetrate cells through endocytosis mechanism. BBR was undetectable in arterial arch tissue of experimental mice, which indicated that the effect of BBR on AS might attribute to its action in the liver and adipose rather than the direct treatment of arterial lesions. Based on these results, we further explored the molecular mechanism and pharmacodynamics of BT₁₅₀₀M on AS. Consistently, the results showed that BT₁₅₀₀M could effectively upregulate p-AMPK expression and downregulate NF- κ B expression in the liver and fat tissues, inhibit the trigger of macrophage activation, and interrupt a crosstalk process between adipocytes and macrophages, leading to improved status of dyslipidemia and inflammation induced by HFD. These results were verified by *in vitro* experiments on PMA-stimulated adipose and LPS-stimulated macrophage cells. The optimal effect of BT₁₅₀₀M probably attributes to its efficacy in improving drug deposition and synergistic effect with the functional carrier TPGS₁₅₀₀. Recently, many studies have been performed to elucidate the effect of BBR on AS, but the underlying mechanism is unclear^{11,52,53}. In the present study, we elucidated, at least in part, the molecular mechanism and pharmacodynamics of the studied drugs based on information on organ distribution. Finally, our results demonstrated that the positive effect of BBR on AS treatment could be magnified by increasing drug absorption and drug-carrier synergism *via* functional biomaterial-based nano technology. However, a BBR nano-system without D- α -tocopherol moiety should be investigated to further elucidate the synergistic anti-atherosclerosis effect of the TPGS carriers and BBR.

5. Conclusions

In this study, three TPGS analogs were synthesized to formulate BBR-entrapped nano-systems for improving the anti-atherosclerotic efficacy of BBR. Our study showed that the nano-system BT₁₅₀₀M could increase gut absorption and intracellular uptake of BBR, leading to increased active drug deposition in the liver and adipose site. In *ApoE*^(-/-) mice, BT₁₅₀₀M intervention (100 mg/kg of BBR) for 5 months ameliorated dyslipidemia and inflammation induced by HFD. Thus, endothelial injury and consequent macrophage activation, cytokine release as well as CE gathering in the aortic arch site improved, resulting in the alleviation of artery plaque build-up. The molecular mechanism study showed that the therapeutic benefit of BT₁₅₀₀M was attributed to its gene-modulating effect and macrophage inhibition. In conclusion, BT₁₅₀₀M shows promise for clinical use in the treatment of AS.

Acknowledgments

This work was supported by the CAMS Innovation Fund for Medical Sciences (No. 2016-I2M-1-011, China); the National Sciences and Technology Major Project (Nos. 2018ZX09711001-003-002, 2017ZX09101003-003-002 and 2016ZX09101017,

China); National Natural Science Foundation of China (No. 81621064); National Key R&D Project (No. 2019YFC170890, China).

Author contributions

Xiaolei Ma, Tingting Zhang, Zhigang Luo, Xiaolin Li, Miao Lin, Rui Li, Peng Du, Xiaoyou Yu, Chen Ma and Pengju Yan performed experiments and analytical methods. Lulu Wang and Yuhuan Li conceived and designed the experiments. Jin Su, Lulu Wang and Yuhuan Li, interpreted and discussed the data, reviewed and edited the manuscript. Lulu Wang and Jiandong Jiang developed the hypothesis, coordinate the project and wrote the manuscript.

Conflicts of interest

The authors have no conflicts of interest to declare.

Appendix A. Supporting information

Supporting data to this article can be found online at <https://doi.org/10.1016/j.apsb.2020.03.005>.

References

1. Aron-Wisnewsky J, Clément K. The gut microbiome, diet, and links to cardiometabolic and chronic disorders. *Nat Rev Nephrol* 2016;**12**: 169–81.
2. Libby P. Mechanisms of acute coronary syndromes and their implications for therapy. *N Engl J Med* 2013;**368**:2004–13.
3. Sénécal M, Fodor G, Gagné C, Genest J, Lavoie MA, McPherson R, et al. Limitations of statin monotherapy for the treatment of dyslipidemia: a projection based on the canadian lipid study-observational. *Curr Med Res Opin* 2009;**25**:47–55.
4. Mansi IA, Mortensen EM, Pugh MJ, Wegner M, Frei CR. Incidence of musculoskeletal and neoplastic diseases in patients on statin therapy: results of a retrospective cohort analysis. *Am J Med Sci* 2013;**345**: 343–8.
5. Pérez de Isla L, Fernández PLS, Álvarez-Sala Walther L, Barrios Alonso V, Castro Conde A, Galve Basilio E, et al. Comments on the 2016 ESC/EAS guidelines for the management of dyslipidemias. *Rev Esp Cardiol* 2017;**70**:72–7.
6. Arnett DK, Blumenthal RS, Albert MA, Buroker AB, Goldberger ZD, Hahn EJ, et al. 2019 ACC/AHA guideline on the primary prevention of cardiovascular disease: executive summary: a report of the American college of cardiology/American Heart Association task force on clinical practice guidelines. *J Am Coll Cardiol* 2019;**74**:1376–414.
7. Zheng SL, Alistair J, Roddick B. Association of aspirin use for primary prevention with cardiovascular events and bleeding events: a systematic review and meta-analysis. *J Am Med Assoc* 2019;**321**: 277–87.
8. Yan TT, Yan NN, Wang P, Xia YL, Hao HP, Wang GJ, et al. Herbal drug discovery for the treatment of nonalcoholic fatty liver disease. *Acta Pharm Sin B* 2020;**10**:3–18.
9. Catapano AL, Graham I, de Backer G, Wiklund O, Chapman MJ, Drexel H, et al. 2016 ESC/EAS guidelines for the management of dyslipidaemias: the task force for the management of dyslipidaemias of the european society of cardiology (ESC) and european atherosclerosis society (EAS) developed with the special contribution of the european association for cardiovascular prevention & rehabilitation (EACPR). *Atherosclerosis* 2016;**253**:281–344.
10. Lan J, Zhao Y, Dong F, Yan Z, Zheng W, Fan J, et al. Meta-analysis of the effect and safety of berberine in the treatment of type 2 diabetes

- mellitus, hyperlipemia and hypertension. *J Ethnopharmacol* 2015;**161**: 69–81.
11. Zimetti F, Adorni MP, Ronda N, Gatti R, Bernini F, Favari E. The natural compound berberine positively affects macrophage functions involved in atherogenesis. *Nutr Metabol Cardiovasc Dis* 2015;**25**: 195–201.
 12. Chang X, Yan H, Fei J, Jiang M, Zhu H, Lu D, et al. Berberine reduces methylation of the mtp promoter and alleviates fatty liver induced by a high-fat diet in rats. *J Lipid Res* 2010;**51**:2504–15.
 13. Zhu L, Zhang DY, Zhu H, Zhu JM, Weng SG, Dong L, et al. Berberine treatment increases *Akkermansia* in the gut and improves high-fat diet-induced atherosclerosis in *Apoe*^{-/-} mice. *Atherosclerosis* 2018;**268**: 117–26.
 14. Gu S, Cao B, Sun R, Tang Y, Paletta JL, Wu X, et al. A metabolomic and pharmacokinetic study on the mechanism underlying the lipid-lowering effect of orally administered berberine. *Mol Biosyst* 2015;**11**: 463–74.
 15. Fan D, Wu X, Dong W, Sun W, Li J, Tang X. Enhancement by sodium caprate and sodium deoxycholate of the gastrointestinal absorption of berberine chloride in rats. *Drug Dev Ind Pharm* 2013; **39**:1447–56.
 16. Zhu JX, Tang D, Feng L, Zheng ZG, Wang RS, Wu AG, et al. Development of self-microemulsifying drug delivery system for oral bioavailability enhancement of berberine hydrochloride. *Drug Dev Ind Pharm* 2013;**39**:499–506.
 17. Cao N, Feng SS. Doxorubicin conjugated to D- α -tocopheryl polyethylene glycol 1000 succinate (TPGS): conjugation chemistry, characterization, *in vitro* and *in vivo* evaluation. *Biomaterials* 2008;**29**: 3856–65.
 18. Collnot EM, Baldes C, Wempe MF, Hyatt J, Navarro L, Edgar KJ, et al. Influence of vitamin E TPGS poly(ethylene glycol) chain length on apical efflux transporters in Caco-2 cell monolayers. *J Contr Release* 2006;**111**:35–40.
 19. Mi Y, Liu Y, Feng SS. Formulation of docetaxel by folic acid-conjugated D- α -tocopheryl polyethylene glycol succinate 2000 (vitamin E TPGS_{2k}) micelles for targeted and synergistic chemotherapy. *Biomaterials* 2011;**32**:4058–66.
 20. Devaraj S, Tang R, Adams-Huet B, Harris A, Seenivasan T, de Lemos JA, et al. Effect of high-dose α -tocopherol supplementation on biomarkers of oxidative stress and inflammation and carotid atherosclerosis in patients with coronary artery disease. *Am J Clin Nutr* 2007;**86**:1392–8.
 21. Zhao J, Feng SS. Effects of PEG tethering chain length of vitamin E TPGS with a Herceptin-functionalized nanoparticle formulation for targeted delivery of anticancer drugs. *Biomaterials* 2014;**35**:3340–7.
 22. Dintaman JM, Silverman JA. Inhibition of P-glycoprotein by D- α -tocopheryl polyethylene glycol 1000 succinate (TPGS). *Pharm Res (N Y)* 1999;**16**:1550–6.
 23. Abu-Fayyad A, Behery F, Sallam AA, Alqahtani S, Ebrahim H, El Sayed KA, et al. PEGylated γ -tocotrienol isomer of vitamin E: synthesis, characterization, *in vitro* cytotoxicity, and oral bioavailability. *Eur J Pharm Biopharm* 2015;**96**:185–95.
 24. Bisht S, Feldmann G, Soni S, Ravi R, Karikar C, Maitra A, et al. Polymeric nanoparticle-encapsulated curcumin (“nanocurcumin”): a novel strategy for human cancer therapy. *J Nanobiotechnol* 2007;**5**:3.
 25. Chen W, Miao YQ, Fan DJ, Yang SS, Lin X, Meng LK, et al. Bioavailability study of berberine and the enhancing effects of TPGS on intestinal absorption in rats. *AAPS PharmSciTech* 2011;**12**: 705–11.
 26. Guo HH, Feng CL, Zhang WX, Luo ZG, Zhang HJ, Zhang TT, et al. Liver-target nanotechnology facilitates berberine to ameliorate cardio-metabolic diseases. *Nat Commun* 2019;**10**:1981.
 27. Murphy JE, Tedbury PR, Homer-Vanniasinkam S, Walker JH, Ponnambalam S. Biochemistry and cell biology of mammalian scavenger receptors. *Atherosclerosis* 2005;**182**:1–15.
 28. Yin Y, Li X, Sha X, Xi H, Li YF, Shao Y, et al. Early hyperlipidemia promotes endothelial activation via a caspase-1-sirtuin 1 pathway. *Arterioscler Thromb Vasc Biol* 2015;**35**:804–16.
 29. Tarakcioglu M, Erbagci AB, Usalan C, Deveci R, Kocabas R. Acute effect of hemodialysis on serum levels of the proinflammatory cytokines. *Mediat Inflamm* 2003;**12**:15–9.
 30. Li CH, Tang SC, Wong CH, Wang Y, Jiang JD, Chen Y. Berberine induces miR-373 expression in hepatocytes to inactivate hepatic steatosis associated AKT-S6 kinase pathway. *Eur J Pharmacol* 2018; **825**:107–18.
 31. Li Z, Jiang JD, Kong WJ. Berberine up-regulates hepatic low-density lipoprotein receptor through Ras-independent but AMP-activated protein kinase-dependent Raf-1 activation. *Biol Pharm Bull* 2014;**37**: 1766–75.
 32. Guo T, Woo SL, Guo X, Li H, Zheng J, Botchlett R, et al. Berberine ameliorates hepatic steatosis and suppresses liver and adipose tissue inflammation in mice with diet-induced obesity. *Sci Rep* 2016;**6**: 22612.
 33. Olefsky JM, Glass CK. Macrophages, inflammation, and insulin resistance. *Annu Rev Physiol* 2010;**72**:219–46.
 34. McNelis JC, Olefsky JM. Macrophages, immunity, and metabolic disease. *Immunity* 2014;**41**:36–48.
 35. Ye L, Liang S, Guo C, Yu X, Zhao J, Zhang H, et al. Inhibition of M1 macrophage activation in adipose tissue by berberine improves insulin resistance. *Life Sci* 2016;**166**:82–91.
 36. Lin WC, Lin JY. Five bitter compounds display different anti-inflammatory effects through modulating cytokine secretion using mouse primary splenocytes *in vitro*. *J Agric Food Chem* 2011;**59**: 184–92.
 37. Xing LJ, Zhang L, Liu T, Hua YQ, Zheng PY, Ji G. Berberine reducing insulin resistance by up-regulating IRS-2 mRNA expression in nonalcoholic fatty liver disease (NAFLD) rat liver. *Eur J Pharmacol* 2011;**668**:467–71.
 38. Combadière C, Potteaux S, Rodero M, Simon T, Pezard A, Esposito B, et al. Combined inhibition of CCL2, CX3CR1, and CCR5 abrogates LY6C^{hi} and LY6C^{lo} monocytosis and almost abolishes atherosclerosis in hypercholesterolemic mice. *Circulation* 2008;**117**:1649–57.
 39. Zhang Y, Li X, Zou D, Liu W, Yang J, Zhu N, et al. Treatment of type 2 diabetes and dyslipidemia with the natural plant alkaloid berberine. *J Clin Endocrinol Metab* 2008;**93**:2559–65.
 40. Jeong HW, Hsu KC, Lee JW, Ham M, Huh JY, Shin HJ, et al. Berberine suppresses proinflammatory responses through AMPK activation in macrophages. *Am J Physiol Endocrinol Metab* 2009;**296**: E955–64.
 41. Kahn BB, Alquier T, Carling D, Hardie DG. AMP-activated protein kinase: ancient energy gauge provides clues to modern understanding of metabolism. *Cell Metabol* 2005;**1**:15–25.
 42. Ouchi N, Shibata R, Walsh K. AMP-activated protein kinase signaling stimulates VEGF expression and angiogenesis in skeletal muscle. *Circ Res* 2005;**96**:838–46.
 43. Zong H, Ren JM, Young LH, Pypaert M, Mu J, Birnbaum MJ, et al. AMP kinase is required for mitochondrial biogenesis in skeletal muscle in response to chronic energy deprivation. *Proc Natl Acad Sci U S A* 2002;**99**:15983–7.
 44. Li J, Zhong LP, Wang FZ, Zhu HB. Dissecting the role of AMP-activated protein kinase in human diseases. *Acta Pharm Sin B* 2017;**7**: 249–59.
 45. Baker RG, Hayden MS, Ghosh S. NF- κ B, inflammation, and metabolic disease. *Cell Metabol* 2011;**13**:11–22.
 46. Wu Y, Huang X, Yang M, Xu J, Chen Z, Yu Z, et al. Ameliorative effect of berberine coated bio-active nanoparticles in acetaminophen induced hepato-renal damage in diabetic rats. *J Photochem Photobiol, B* 2018;**189**:250–7.
 47. Hu JP, Nishishita K, Sakai E, Yoshida H, Kato Y, Tsukuba T, et al. Berberine inhibits RANKL-induced osteoclast formation and survival through suppressing the NF- κ B and Akt pathways. *Eur J Pharmacol* 2008;**580**:70–9.
 48. Li C, Wang J, Wang Y, Gao H, Wei G, Huang Y, et al. Recent progress in drug delivery. *Acta Pharm Sin B* 2019;**9**:1145–62.
 49. Mu L, Elbayoumi TA, Torchilin VP. Mixed micelles made of poly(ethylene glycol)-phosphatidylethanolamine conjugate and

- D- α -tocopheryl polyethylene glycol 1000 succinate as pharmaceutical nanocarriers for camptothecin. *Int J Pharm* 2005;**306**:142–9.
50. Dabholkar RD, Sawant RM, Mongayt DA, Devarajan PV, Torchilin VP. Polyethylene glycol–phosphatidylethanolamine conjugate (PEG-PR)-based mixed micelles: some properties, loading with paclitaxel, and modulation of P-glycoprotein-mediated efflux. *Int J Pharm* 2006;**315**:148–57.
51. Kutty RV, Chia SL, Setyawati MI, Muthu MS, Feng SS, Leong DT. *In vivo* and *ex vivo* proofs of concept that cetuximab conjugated vitamin E TPGS micelles increases efficacy of delivered docetaxel against triple negative breast cancer. *Biomaterials* 2015;**63**:58–69.
52. Liu Y, Liu X, Hua W, Wei Q, Fang X, Zhao Z, et al. Berberine inhibits macrophage M1 polarization via AKT1/SOCS1/NF- κ B signaling pathway to protect against DSS-induced colitis. *Int Immunopharm* 2018;**57**:121–31.
53. Li K, Yao W, Zheng X, Liao K. Berberine promotes the development of atherosclerosis and foam cell formation by inducing scavenger receptor a expression in macrophage. *Cell Res* 2009;**19**:1006–17.